Advanced Fiber Characterization Technologies for Fiber Lasers and Amplifiers

Andrew D. Yablon
Interfiber Analysis, 8 Manns Hill Crescent, Sharon, MA 02067, USA
andrew_yablon@interfiberanalysis.com

Abstract: Optical fiber gain profiling, spectrogram modal analysis, and interferometric refractive index and residual stress measurement are presented. Information obtained from these novel characterization technologies is critical for design and assembly of fiber-based lasers and amplifiers.

OCIS codes: (060.2270) Fiber Characterization; (060.3510) Lasers, fiber

1. Introduction

The rapid development of high-power fiber lasers and amplifiers during the past decade has created a need for new technologies for characterizing fibers and fiber devices. Examples discussed here include novel techniques for measuring the refractive index profile and geometry of fibers, methods to measure a fiber's residual stress profile or the spatial distribution of a fiber's gain dopant distribution, and quantification of the modal content of few-mode optical fibers and devices. Rapid commercialization of these technologies during the past few years have ensured that they are available for optimizing high-power fibers and fiber laser assemblies, qualifying components, and understanding impairments in applications ranging from research to product development to manufacturing.

2. Refractive Index

The most important parameter controlling the performance of an optical fiber is its refractive index distribution, which determines the properties of any guided modes. Transverse interferometry is a particularly powerful approach to quantifying this refractive index distribution because it can be applied to a thin cross sectional slice of an uncleaved fiber at a variety of measurement wavelengths [1] and can be used to optimize fusion splices or fiber interconnections [2,3]. Since no cleave is required, changes to the fiber's index profile along the axial direction can be mapped out, for example in tapered fiber or grating. In transverse interferometry the fiber is positioned in one arm of a single-pass Mach-Zehnder interferometer. The probe beam passes across the fiber rather than along the fiber's axis. In addition to traditional doped-silica glass, unusual fiber materials such as fluoride glasses, phosphate glasses, sapphire, or even polymers can be measured this way. Transverse interferometry was recently employed to measure a fiber's refractive index profile across wavelengths spanning more than 2.5 octaves, from about 370 nm to about 2000 nm [4], thereby illustrating that transverse interferometry can measure the refractive index profile of high-power laser fibers and amplifiers at or near their operating bands (1060 nm, 1550 nm, 2000 nm, etc.).

3. Tomography

When a fiber is not azimuthally symmetric, reconstruction of the complete two-dimensional fiber cross section requires the incorporation of transverse projection data acquired from a multiplicity of rotational angles. Traditionally this combination is performed using filtered backprojection, a convenient numerical implementation of the inverse Radon transform. In order to achieve fine spatial resolution, a fiber sample must be imaged with high numerical aperture objective lenses whose depth of field is approximately two orders of magnitude smaller than the transverse width of typical fibers. In the presence of this constraint, conventional filtered backprojection produces significant measurement artifacts, especially for features far from the fiber's center axis [5]. A newly described multifocus tomographic algorithm overcomes this limitation and achieves fine spatial resolution (~1 µm) over large transverse distances (~100 µm) [5,6]. In this case, projection data is acquired at a multiplicity of focal positions and also at a multiplicity of angular orientations. A full three-dimensional measurement of the variation of an optical fiber cross section along the length of the fiber can be assembled from a large number of discrete two-dimensional cross sections computed at distinct axial locations along the fiber [3].

4. Residual Stress and Strain

Residual stresses and strains in an optical fiber can produce significant optical effects in fiber lasers and amplifiers [7,8] . Sufficiently precise measurements of the refractive index profile, taken with probe light of appropriate polarization, can be used to compute the residual axial stress in the fiber [9]. When appropriate, filtered

backprojection or the new multifocus algorithm can be combined to provide a complete two-dimensional residual axial stress cross-section of the fiber sample. Transverse interferometry can provide three-dimensional representations of a residual stress state that changes near a fusion splice or cleave. Figure 1 depicts typical one-dimensional and two-dimensional tomographic refractive index profiles and residual axial stress profiles. Spatial resolution is evidently on the order of one micron whereas the noise floor is seen to be on the order of one MPa. The blue trace is a Tm-doped fiber designed for 2000 nm operation with an approximately 25 micron diameter inner core surrounded by a an approximately 45 micron diameter pedestal. It is seen that the pedestal induces a substantial amount of tensile axial residual stress, which primarily results from the fact that the heavily doped pedestal region has a much larger thermal expansion coefficient than the surrounding silica glass and therefore is unable to fully contract during cooling. The green trace, *Corning Clearcurve ZBL*, is a low-bend loss single-mode fiber with a deeply down-doped trench surrounding the core. This trench is presumably doped with fluorine and it is seen that such doping induces strong compressive residual axial stress. The false color two-dimensional tomographic refractive index and residual stress polarization-maintaining (PM) fiber measurements are seen to achieve micron-scale spatial resolution and can detect the micron-sized central dip in the middle of the fiber's core.
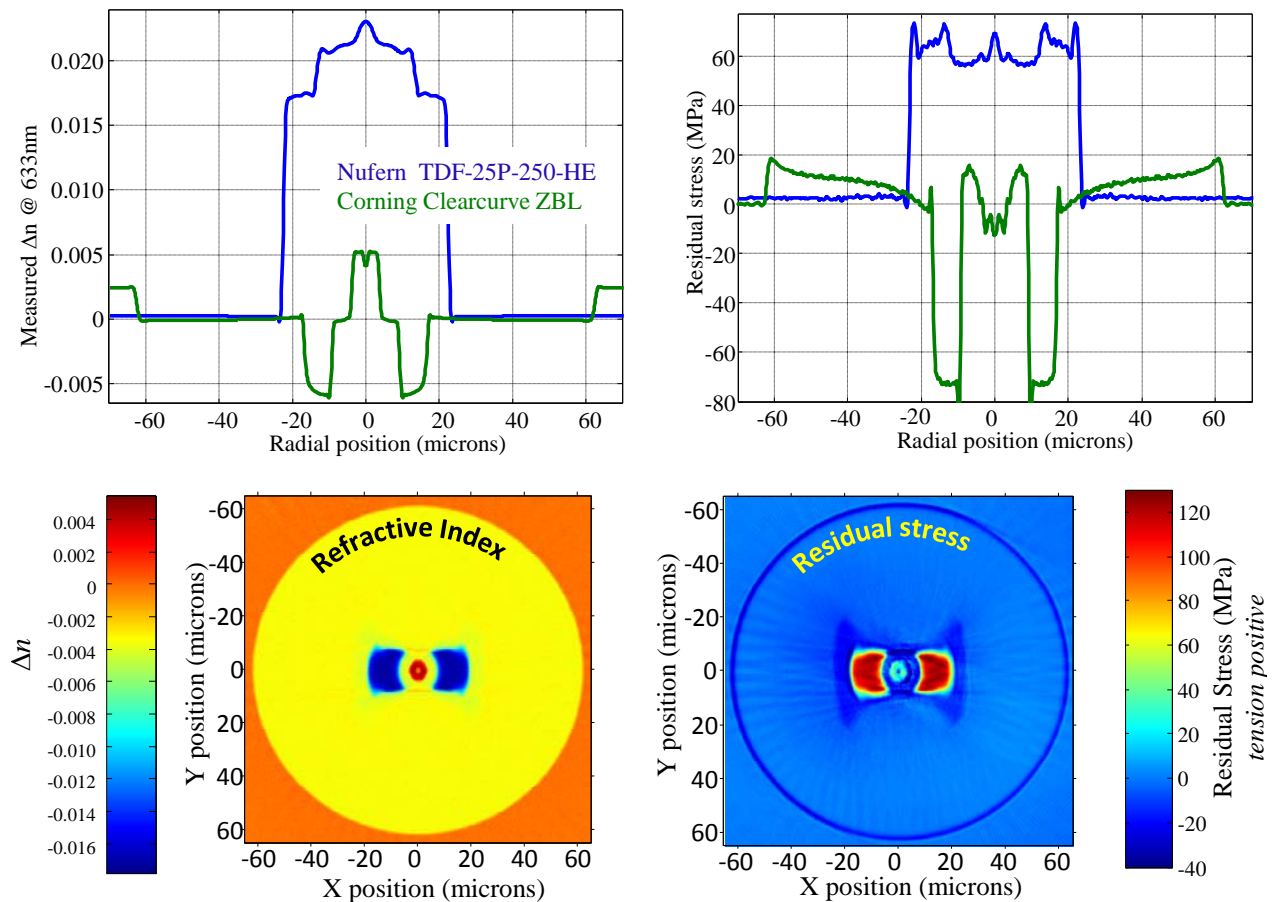
Fig. 1. Refractive index profiles for two axisymmetric fiber samples measured at 633 nm (*top left*) contrasted with (*top right*) corresponding residual axial stress profiles on the same two fiber samples [10]. False color two-dimensional refractive index map measured on a non-axisymmetric PM fiber (*bottom left*) contrasted with (*bottom right*) corresponding false color two-dimensional residual stress profile. PM fibers are courtesy *Fibercore Ltd.*

5. Spatial Gain Profiling

Gain fibers may benefit from a deliberately inhomogeneous distribution of rare-earth dopants, and hence gain [11], while photodarkening has been found to be spatially inhomogeneous [12]. Therefore, the spatial distribution of a fiber's gain is important and can be measured by pumping the fiber transversely through its side at a suitable wavelength with a homogeneous plane wave while measuring the spontaneous emission transversely through the side of the fiber [3]. In this way, the wave guiding characteristics of the fiber's modes will not

contribute to the measured signal and therefore can be ignored. Instead, the spatial variation in the spontaneous emission is directly attributable to the spatial distribution of rare-earth dopant and gain in the fiber. Optical pumping is accomplished with a single-mode fiber carrying an appropriate laser signal inserted into an oil bath to produce a homogeneous plane wave excitation across the entire gain fiber. The spontaneous emission from Yb-doped silica fibers can be detected with silicon CCD array detectors whereas the spontaneous emission from Ho- and Tm-doped silica fibers can be detected with suitable mid-IR infrared array detectors, such as InGaAs or HgCdTe.

6. Modal Content

M^2 has been shown to be poorly suited to characterizing fiber lasers and amplifiers [13]. A tunable laser combined with an array detector can be used to identify and quantify higher order modes in a high-power large-mode-area (LMA) fiber, or fiber component, via a spectrogram approach [14]. Figure 2 shows sample data acquired on a typical LMA fiber when energy is launched from a single-mode fiber without any special mode matching. Coupling to higher-order modes at a discrete location, for example at an interconnection or fusion splice, can be distinguished from distributed mode coupling, for example resulting from fiber packaging. The intermodal dispersion and relative modal power is quantifiable with this approach. Both the intensity and phase distribution of higher order modes can be precisely measured as shown in Figure 2, thereby conclusively identify the mode. Quantitative assessment of the actual modal content permits a much clearer understanding of the emitted beam quality and how to improve it.
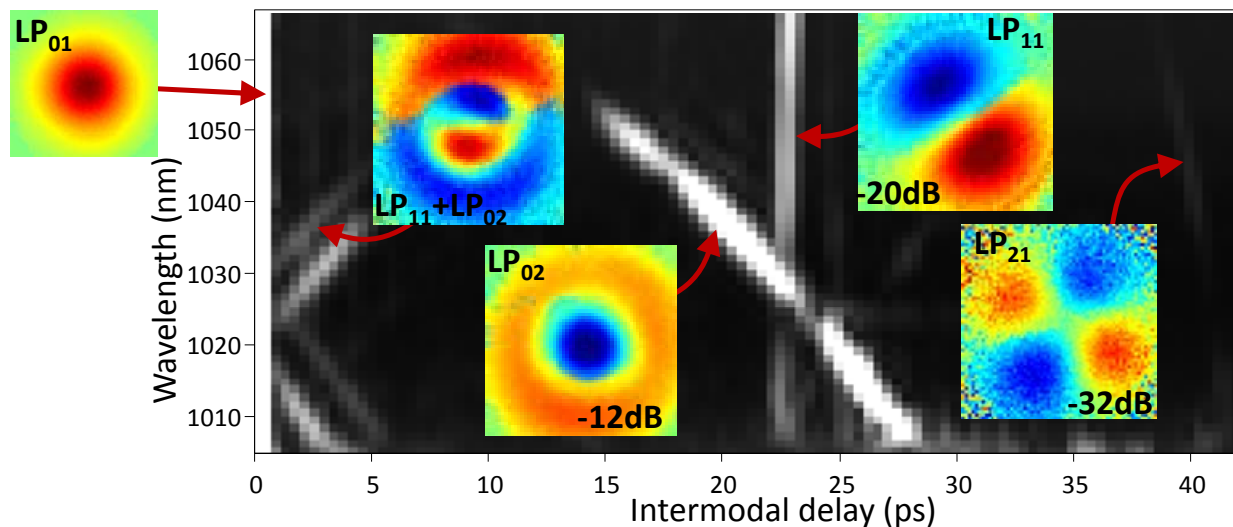

Fig. 2. Sample spectrogram data acquired on a 20 µm core diameter low-NA few-mode LMA fiber directly spliced to a single-mode fiber. The false color inserts depicts measured electric field magnitudes of various low-order modes where red is positive electric field and red is negative electric field. The identity and relative power of various higher-order modes is readily apparent from the spectrogram data.

7. References

[1] A. D. Yablon, IEEE J of Lightwave Technol **28**, 360-365 (2010).

[2] A. D. Yablon, *Optical Fiber Fusion Splicing*, (Springer, New York, 2005).

[3] A. D. Yablon, Opt Engineering **50**, 11603 (2011).

[4] A. D. Yablon and J. Jasapara, "Hyperspectral optical fiber refractive index measurement spanning 2.5 octaves", Proc. SPIE 8601, (2013)

[5] A. D. Yablon, Opt Lett **38**, 4393-4396 (2013).

[6] A. D. Yablon, "Novel multifocus tomography for measurement of microstructured and multicore optical fibers," Proc. SPIE 8961 (2014).

[7] F. Just *et al*, IEEE J of Lightware Technol **27**, 2111-2116 (2009).

[8] L. Fu, *et al*, Opt Express **17**, 11782-11793 (2009).

[9] M. P. Varnham, e*t al*, Electron Lett **20**, 1034-1035, (1984).

[10] A. D. Yablon, 1st International Meeting on Fiber Lasers and Applications, June 22-23, 2014, Bar-Ilan University, Ramat Gan, Israel.

[11] R. S. Quimby *et al* IEEE J of Sel Topics in Quantum Electronics **15**, 12-18 (2009).

[12] M. J. Söderlund *et al*, Opt Express **16**, 10633-10640 (2008).

[13] S. Wielandy, Opt. Express **15**, 15402-15409 (2007).

[14] J. Jasapara, and A. D. Yablon, Opt Lett **37**, 3906-3908 (2012).